AGU PUBLICATIONS

Geophysical Research Letters

RESEARCH LETTER
10.1002/2014GL061362

Key Points:
- With weak pPv, cold slabs spread more easily and broadly along the CMB
- This increases the CMB heat flux and the steepness of the primordial reservoirs
- The stability of primordial reservoirs is not substantially altered by weak pPv

Correspondence to:
Y. Li,
yang.li@erdw.ethz.ch

Citation:
Li, Y., F. Deschamps, and P. J. Tackley (2014), Effects of low-viscosity post-perovskite on the stability and structure of primordial reservoirs in the lower mantle, *Geophys. Res. Lett.*, *41*, 7089–7097, doi:10.1002/2014GL061362.

Received 31 JUL 2014
Accepted 19 SEP 2014
Accepted article online 23 SEP 2014
Published online 24 OCT 2014

Effects of low-viscosity post-perovskite on the stability and structure of primordial reservoirs in the lower mantle

Yang Li[1], Frédéric Deschamps[2], and Paul J. Tackley[1]

[1]Institute of Geophysics, ETH Zurich, Zurich, Switzerland, [2]Institute of Earth Sciences, Academia Sinica, Taipei, Taiwan

Abstract We performed numerical experiments of thermochemical convection in 3-D spherical geometry to investigate the effects of a low viscosity of post-perovskite (pPv) on the stability and structure of primordial reservoirs of dense material in the lower mantle of the Earth. Our results show that weak pPv (1000 × viscosity reduction in regions containing pPv) strongly increases the core-mantle boundary (CMB) heat flux. The volume-averaged mantle temperature with weak pPv is slightly higher than that with regular pPv, except in the lowermost mantle. This is because weak pPv weakens the base of the cold downwellings, allowing cold slabs to spread more easily and broadly along the CMB. The stability and size of the dense reservoirs is not substantially altered by weak pPv. In the weak pPv case, slabs spreading along the CMB slightly decreases the stability of dense reservoirs, i.e., the amount of dense material entrained upward is slightly larger than in the regular pPv case (i.e., viscosity of pPv identical to that of perovskite). Furthermore, the topography and steepness of these reservoirs slightly increase. However, as in the regular pPv case, the dense reservoirs are maintained over periods of time comparable to the age of the Earth.

1. Introduction

Sidorin et al. [1999] first suggested that a strong exothermic phase transition, which would be deflected upward by low temperatures, fits the seismological observations in the *D″* region better than a chemical boundary. Such an exothermic phase transition from perovskite (Pv) to post-perovskite (pPv) was subsequently discovered by *Murakami et al.* [2004], *Tsuchiya et al.* [2004], and *Oganov and Ono* [2004] under similar temperature and pressure conditions as the Earth's deep mantle. This phase change also has a strongly positive Clapeyron slope, which may be as high as 13 MPa/K [*Tateno et al.*, 2009; *Hernlund*, 2010]. The presence of post-perovskite is needed to explain P_{diff} and S_{diff} arrivals [*Cobden et al.*, 2012]. It has been suggested that it may further explain the lowermost mantle seismic tomography [*Davies et al.*, 2012]. Other studies, however, indicate that compositional anomalies are further needed to fully explain seismic tomography [*Deschamps et al.*, 2012; *Mosca et al.*, 2012]. Furthermore, pPv is expected to be highly anisotropic which may explain seismic anisotropy observed at the bottom of the mantle [e.g., *Wookey et al.*, 2005]. First, principle calculations of atomic diffusion [*Ammann et al.*, 2010] indicate that the viscosity of post-perovskite may be lower than that of perovskite by a factor of $O(10^3)$ to $O(10^4)$. Dynamically, the combination of a low viscosity and a large positive Clapeyron slope should have some influences on the long-term evolution of thermal and chemical structures in the mantle.

Compositional heterogeneities are widely thought to exist above the core-mantle boundary (CMB) in order to explain observations from various global seismological studies [e.g., *Ishii and Tromp*, 1999; *Masters et al.*, 2000; *Trampert et al.*, 2004] and local regional seismological studies [e.g., *Ni et al.*, 2002; *Wang and Wen*, 2007; *He and Wen*, 2012]. The detailed nature of these compositional heterogeneities is still not clearly understood. One hypothesis is that they are reservoirs of primordial material formed at early stages in the Earth's history through one or more melting-related differentiation processes [e.g., *Solomatov and Stevenson*, 1993; *Labrosse et al.*, 2007; *Lee et al.*, 2010] and that these primordial reservoirs have been maintained in the lower mantle over the Earth's history with limited interaction with the surface. The presence of undegassed reservoirs in the deep mantle is further supported by oceanic island basalts geochemistry (see *Hofmann* [1997] for a review). Previous numerical experiments have identified important parameters controlling the stability of dense reservoirs [e.g., *McNamara and Zhong*, 2005; *Deschamps and Tackley*, 2008, 2009; *Li et al.*, 2014], including the buoyancy ratio and the thermal viscosity contrast. These studies, however, did not include the Pv to pPv phase transition.

Other studies have focused on the influence of weak pPv on mantle convection [e.g., *Nakagawa and Trackley*, 2011; *Samuel and Tosi*, 2012; *Li and McNamara*, 2013] and found important effects, in particular a higher mantle temperature, a higher CMB heat flux, and smaller CMB topography. However, no studies have investigated the dynamical influence of weak pPv on the stability and structure of primordial reservoirs of dense material in the lower mantle. Here we use numerical thermochemical mantle convection simulations in a 3-D spherical shell to investigate the stability and structures of these primordial reservoirs of dense material.

2. Methods and Model Setup

The numerical experiments are performed with StagYY [*Tackley*, 2008], which solves the conservation equations of mass, momentum, energy, and composition for an anelastic, compressible fluid with infinite Prandtl number. Calculations are performed in 3-D spherical geometry on the Yin-Yang grid [*Kageyama and Sato*, 2004] with a ratio between inner and outer radii of $f = 0.55$, matching the Earth's mantle.

To model the perovskite to post-perovskite phase transition, we use a phase function approach, which is based on that in *Christensen and Yuen* [1985], defined as

$$\Gamma_{\mathrm{pPv}}(T,z) = 0.5 + 0.5\tanh\frac{z - z_{\mathrm{pPv}} - \gamma_{\mathrm{pPv}}(T - T_{\mathrm{pPv}})}{w} \tag{1}$$

where Γ_{pPv} is the phase function for post-perovskite, which varies from 0 for perovskite to 1 for post-perovskite, T and z are temperature and depth, respectively, $(T_{\mathrm{pPv}}, z_{\mathrm{pPv}})$ is a point on the phase boundary, γ_{pPv} is the Clapeyron slope (which we fix here to 13 MPa/K), and w is the width of the phase transition. In this study, the phase boundary from perovskite to post-perovskite occurs at 2650 K and 2700 km depth, which allows a double crossing in the lowermost mantle [e.g., *Hernlund et al.*, 2005].

The viscosity is assumed to depend on temperature, depth, and yield stress. An additional viscosity jump of 30 is imposed at the boundary between upper and lower mantle. The viscosity is further allowed to depend on the phase (perovskite or post-perovskite). Viscosity is thus given by

$$\begin{aligned}\eta(z,T,\Gamma_{\mathrm{pPv}}) &= \eta_0[1 + 29H(z - 660)]\exp\left[\Gamma_{\mathrm{pPv}}\ln(\eta_{\mathrm{pPv}}) + V_a\frac{z}{D} + E_a\frac{\Delta T_S}{(T + T_{\mathrm{off}})}\right]\\ \eta_Y &= \frac{\sigma_0 + \sigma_i P}{2\dot{e}}\\ \eta &= \frac{1}{\left(\frac{1}{\eta_{(z,T,\Gamma_{\mathrm{pPv}})}} + \frac{1}{\eta_Y}\right)}\end{aligned} \tag{2}$$

where η_0 is the reference viscosity (taken at temperature $T = 1600$ K and depth $z = 0$ km), H is the Heaviside step function, and η_{pPv} is the viscosity jump between perovskite and post-perovskite (1 for regular pPv, and 1/1000 for weak pPv in this study). V_a and E_a are, respectively, the nondimensional activation volume and energy, which control viscosity variations with depth and temperature. In this study, we fixed the value of V_a to 4.602 and E_a to 23.026. T_{off} is the offset temperature which is set to $0.88\Delta T_S$. The yield stress (σ_0) at surface is 300 MPa, and the gradient of yield stress (σ_i) is 0.001 Pa/Pa. Finally, $\dot{e}$ is the second invariant of the strain rate tensor. To avoid numerical difficulties, the viscosity is truncated between 10^{-3} and 10^5 of the reference viscosity.

The reference Rayleigh number is defined as follows:

$$Ra_{\mathrm{ref}} = \frac{\alpha_s g \rho_s \Delta T_s D^3}{\eta_0 \kappa_s} \tag{3}$$

where α_s is the surface thermal expansion, g the acceleration of gravity, ΔT_s the superadiabatic temperature difference, D the mantle thickness, η_0 the reference thermal viscosity (1.6×10^{21} Pa S in this study, which is the viscosity obtained using the potential temperature of 1600 K, and depth of 0 km), and κ_s the surface thermal diffusivity. This reference Rayleigh number remains constant during the entire experiment. In this study we prescribed $Ra_{\mathrm{ref}} = 10^8$. The effective Rayleigh number Ra_{eff} calculated with volume-averaged properties varies with time but remains around 3×10^6.

The initial temperature is adiabatic with a potential temperature of 2000 K, plus thermal boundary layers at top and bottom (300 K at the top and 3750 K at the CMB), and the shell is heated from both the bottom and

Table 1. Mantle Model Physical Parameters

Parameter	Symbol	Value	Units	Nondimensional
Reference Rayleigh number	Ra_s			10^8
Buoyancy ratio	B			0.36
Volume fraction of primordial material	X			0.037
Initial thickness of primordial layer	h_{DL}			0.07
Gravitational acceleration	g	9.81	m/s^2	1.0
Mantle thickness	D	2891	km	1.0
Ratio of inner to outer radii of the shell	f			0.55
Superadiabatic temperature difference	ΔT_S	2500	K	1.0
Reference adiabat	T_{as}	1600	K	0.64
Surface density	ρ_S	3300	kg/m^3	1
CMB density	ρ_b	4950	kg/m^3	1.5
Surface thermal expansion	α_S	5.0×10^{-5}	K^{-1}	1.0
CMB thermal expansion	α_S	1.0×10^{-5}	K^{-1}	0.2
Surface thermal diffusivity	κ_S	6.24×10^{-7}	m^2/s	1.0
CMB thermal diffusivity	κ_b	8.74×10^{-7}	m^2/s	1.4
Reference thermal viscosity ($T = 1600\ K, z = 0\ km$)	η_0	1.6×10^{21}	Pa s	1.0
Reference transition depth (pv-pPv)	z_{pPv}	2700	km	0.934
Reference transition temperature (pv-pPv)	T_{pPv}	2650	K	1.06
Clapeyron slope (pv-pPv)	Γ_{pPv}	13	MPa/K	0.347

within. The numerical resolution is $64 \times 192 \times 64 \times 2$, radially refined in the top and bottom 150 km, with 24 million tracers to track composition. The compositional field is calculated from the fraction of dense tracers at each location and varies between 0 for regular material and 1 for primordial material.

The density contrast between primordial and regular material is controlled by the buoyancy ratio (B)

$$B = \frac{\Delta\rho_C}{\alpha_s \rho_s \Delta T_s} \tag{4}$$

where $\Delta\rho_C$ is the density difference between the dense and regular material. We fix B to 0.36 in this study. For a superadiabatic temperature difference $\Delta T_S = 2500\ K$ and thermal expansion $\alpha_s = 5.0 \times 10^{-5}$ (i.e., taken at $z = 0$ km and $T = 1600$ K), this corresponds to a density contrast of 147 kg/m^3, which, taking preliminary reference Earth model as a reference, leads to a relative density anomaly of about 3% at the bottom of the mantle, in agreement with current estimates of density anomalies in the lower mantle [e.g., *Trampert et al.*, 2004; *Mosca et al.*, 2012]. The values of other physical parameters are listed in Table 1. These values were identified by *Li et al.* [2014] as reasonable values for the Earth mantle, i.e., they lead to long-lived reservoirs of dense material at the bottom of the shell.

To estimate the degree of mixing between dense and regular materials, we used the average depth of dense material, as defined in *Deschamps and Tackley* [2008]:

$$< h_c >= \frac{1}{V}\int_V C(r,\theta,\phi) \mathrm{rdV} \tag{5}$$

For stable layering, $< h_c >$ remains constant in time at $a \times h_{DL}$, where a is a geometrical constant depending on the curvature of the shell and h_{DL} is the initial thickness of the dense layer. As the layer becomes unstable, $< h_c >$ increases. More importantly, $< h_c >$ is a good measure of the degree of mixing of the system at each stage of the experiment. For a ratio between the inner and outer radii of $f = 0.55$, stable layering and efficient mixing lead to $< h_c >$ around 0.04 and 0.63, respectively. Intermediate values indicate the presence of stable reservoirs.

3. Results

To study the influence of the low viscosity of post-perovskite, we performed two experiments, one with $\eta_{pPv} = 1$ (regular pPv) and one with $\eta_{pPv} = 10^{-3}$ (weak pPv). Figure 1 plots the time variations of several output observables of these models. In the weak pPv case, the CMB heat flux is larger by about 50% than in the regular pPv case, in agreement with previous studies in 2-D Cartesian [*Cizkova et al.*, 2010] and 3-D-spherical [*Nakagawa and Tackley*, 2011] geometries. In contrast, in the time range 1.5–4.5 Gyr, the surface heat flux is similar for weak and regular pPv cases, around 55 mW/m^2. In the weak pPv case, the CMB

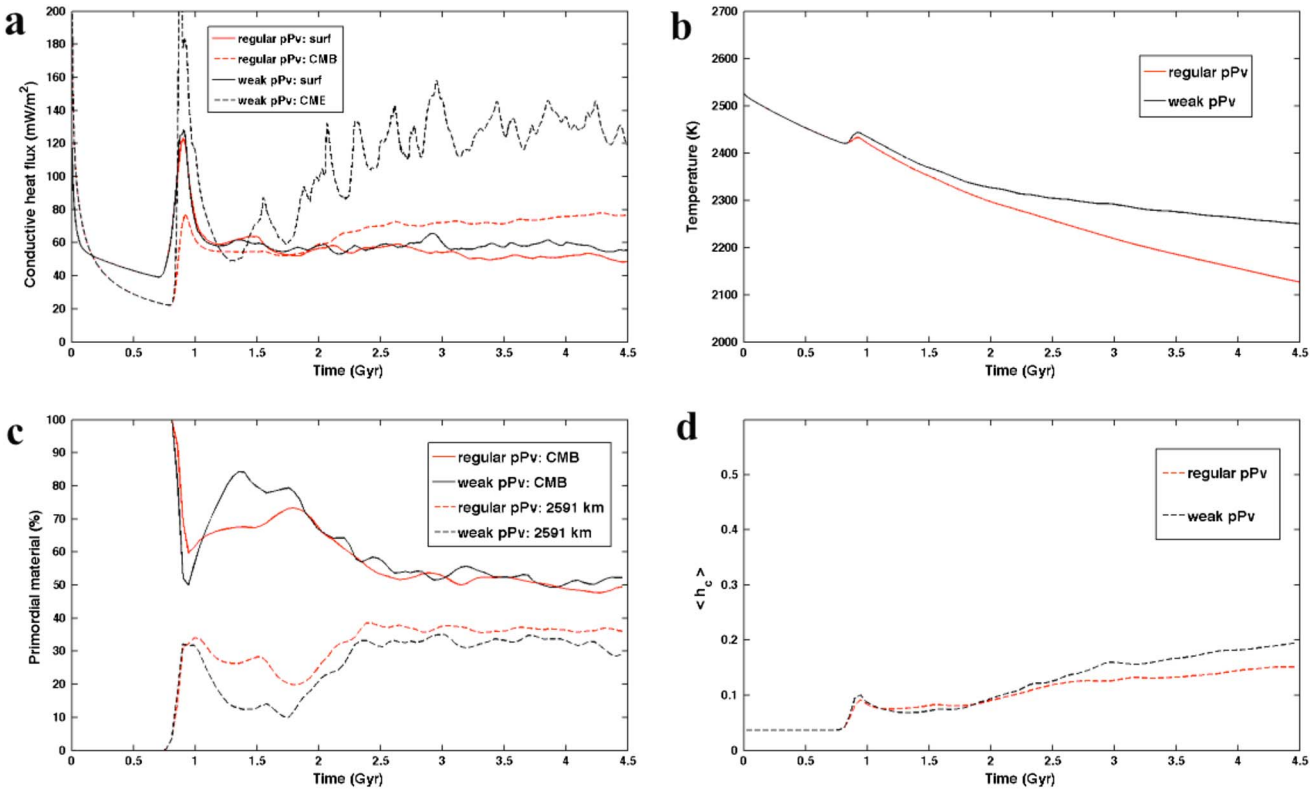

Figure 1. (a) CMB and surface heat flux for regular and weak pPv as a function of time. (b) Volume-averaged mantle temperature as a function of time. (c) Percentage of CMB area and 300 km above CMB area covered by primordial reservoirs as a function of time. (d) The average altitude of primordial material as a function of time.

heat flux is strongly time dependent, with variations of up to 40 mW/m^2 in amplitude and a pseudo-period of around 0.5 Gyr. Such variations are a good indication that strong, small-scale thermal instabilities are generated in the bottom thermal boundary layer. The main explanation for the difference in heat flux between regular and weak pPv cases is that cold slabs can spread more easily over the CMB. Meanwhile, the less time-dependent surface heat flux of both regular and weak pPv cases indicates that the system has reached a statistically steady state. Another interesting difference between the regular and weak pPv cases is that the difference between the CMB and surface heat flux is much larger in the weak pPv case (around 60 mW/m^2) than in the regular pPv case (around 20 mW/m^2). Figure 1b shows the volume-averaged mantle temperature as a function of time, indicating a slower cooling of mantle temperature in the weak pPv case than in the regular pPv case. Figure 1c shows the area covered by primordial reservoirs at CMB and 300 km above CMB with regular and weak pPv. We do not observe significant differences between the regular and weak pPv cases. The area covered by primordial reservoirs at the CMB is similar for the regular and weak pPv cases (around 50%), but at 300 km above CMB, where most of the area is dominated by perovskite, it is slightly large for the regular pPv case (around 35%) than for the weak pPv case (around 30%), indicating that the volume of the dense reservoirs is slightly smaller in the weak pPv case. Figure 1d, showing the average altitude of dense material as a function of time $< h_c >$ (equation (4)), indicates that the reservoirs are stable for both regular and weak pPv cases. Note that $< h_c >$ is slightly larger for the weak pPv case, i.e., the entrainment of dense material by plumes is slightly larger in the weak pPv case. It is important to point out that the difference in the size of the reservoirs and in the entrainment of dense material, as seen by Figures 1c and 1d, remains limited, and overall, the size of the dense reservoirs and the entrainment for the weak and regular pPv case are very similar. We do not see substantial lateral variation in the shape and position of the dense reservoirs. Once formed, the boundaries of reservoirs change slightly with time, but reservoirs remain around the stable around the same location.

Figure 2 shows snapshots of the temperature and composition fields, and the phase boundary of pPv at $t = 4.0$ *Gyr*. As previously indicated by Figure 1c, isosurfaces of the chemical field show that the total CMB

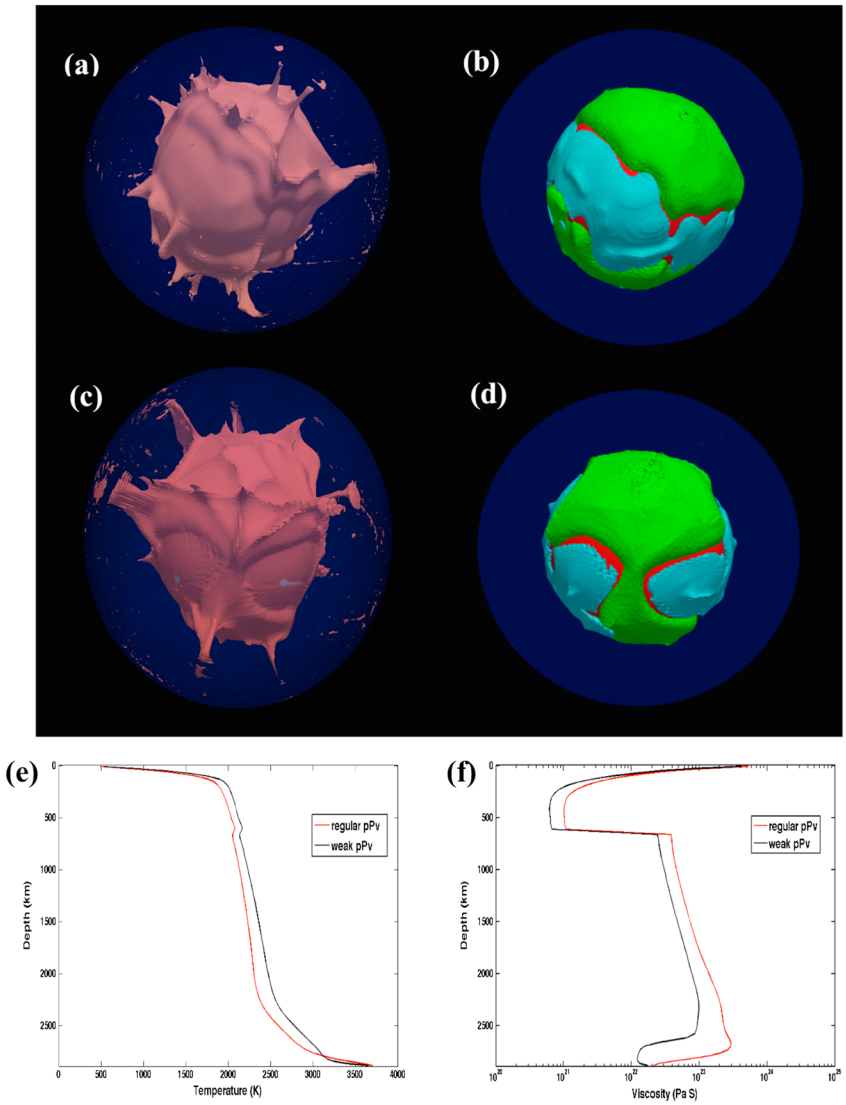

Figure 2. Snapshots of cases with (a, b) regular pPv and (c, d) weak pPv at 4 Gyr. Isosurface of potential temperature with contour level $T = 0.7$ (Figures 2a and 2c). Isosurface of the composition with contour level $C = 0.50$ (green) and isosurface of pPv (cyan) (Figures 2b and 2d). (e) One-dimensional profile of temperature. (f) One-dimensional profile of viscosity for these two cases.

areas covered by primordial reservoirs are similar in these two cases. Figures 3b and 3e further indicate that the topography of the dense reservoirs in the weak and regular pPv cases are comparable. In addition, in both cases the thermal anomalies and the dense reservoirs have steep edges, which is consistent with seismological observations of Large Low Shear Velocity Provinces [*Ni et al.*, 2002]. Note that in both cases, the pPv phase is stable only outside the dense reservoirs, which are hotter than average, and thus outside the stability field of pPv. Since the weak pPv also destabilizes the lower mantle's thermal boundary layer, large plumes arise more easily from the lower thermal boundary layer and are more likely to arise from the margins of the primordial reservoirs, which is consistent with the paleomagnetic reconstruction of the location of large igneous provinces [*Torsvik et al.*, 2006; *Burke et al.*, 2008]. Comparison between the 1-D profiles of temperature shows that the case with weak pPv has a higher average temperature throughout most of the mantle, except in the deepest mantle, where the phase transition from Pv to pPv is most likely to occur. As a consequence, in the case with regular pPv the mantle is globally more viscous throughout the domain. In the case with weak pPv, we further observe a wider spreading of cold downwellings along the CMB area. As a result, in cold regions, the location of the phase transition is shallower than that in the case with regular pPv. This leads to a more heterogenous distribution of pPv in the deep mantle, which may partly help to

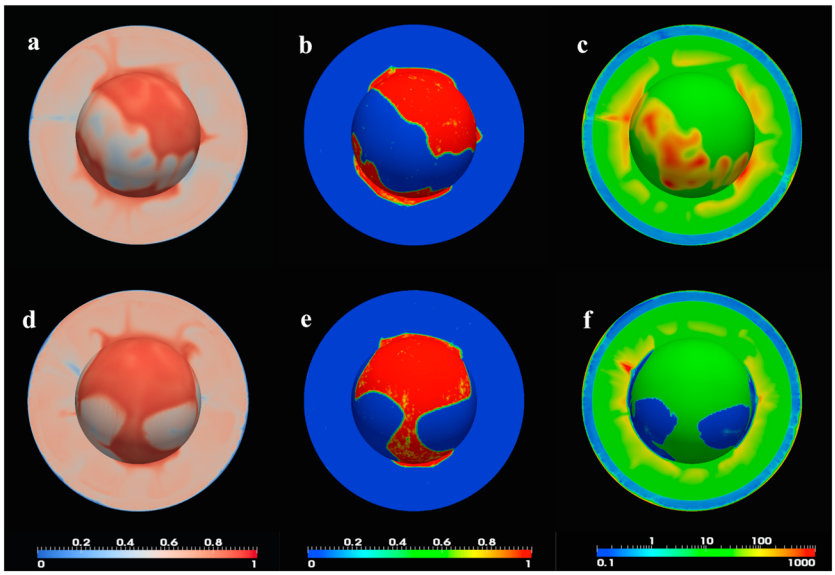

Figure 3. Snapshots of cases with (a–c) regular and (d–f) weak pPv at 2790 km depth and evolution time equals to 4 Gyr. Temperature (Figures 3a and 3d), composition (Figures 3b and 3e), and viscosity (Figures 3c and 3f).

explain the seismic discontinuity in the *D*′′ region. Since the CMB temperature is fixed at 3750 K in this study, the CMB region is still in the stability field of perovskite, and a "double crossing" of the pPv phase change can be observed just above CMB. In the case of weak pPv, this induces a sharp increase in viscosity right above the CMB in a layer of a few tens of kilometers thick (Figure 2f).

Figure 3 shows polar slices of temperature, composition, and viscosity combined with spherical surface slices at 2790 km. Temperature and composition fields at this depth do not have significant differences compared to each other. In contrast, the viscosity field at this depth is different. In the regular pPv case, the dense reservoirs are less viscous than the surrounding material by about 2 orders of magnitude. In the weak pPv case, the situation is reversed, i.e., the reservoirs of dense material are more viscous than the surrounding material (which is mostly in the pPv phase) by 2 orders of magnitude. This leads to a larger topography and sharper edges of the primordial reservoirs.

Figure 4 shows spectral heterogeneity maps of the composition and temperature fields at 4 Gyr for the two experiments. In both cases, chemical heterogeneities are dominated by long-wavelength structure (degree 2) at the bottom of the shell. Because small fractions of dense material are entrained upward by plumes, small-scale heterogeneities may be present elsewhere in the mantle, but Figure 4 shows that these are not significant. Thermal anomalies are dominated by strong degree 2 anomalies in the deep mantle

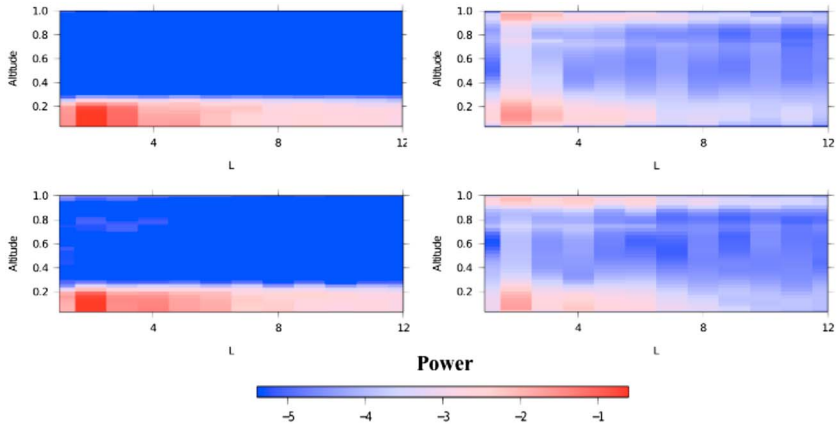

Figure 4. Spectral heterogeneity maps of Figure 2. (top) Regular pPv and (bottom) weak pPv. (left) Composition field and (right) temperature field.

and below the surface. Overall, these heterogeneities would result in strong large-scale seismic velocity anomalies at the bottom of the mantle, as observed in tomographic models, with shear wave velocity in hot reservoirs of dense material appearing slower than average. In our case, the seismic dichotomy between the dense reservoirs and their surroundings would be enhanced by the fact that shear waves travel faster in pPv than in Pv [e.g., *Tsuchiya et al.*, 2004].

4. Discussion

Our calculations show that the presence of weak pPv, with viscosity lower by 3 orders of magnitude compared to Pv, does not substantially modify the stability of reservoirs of dense material at the bottom of the mantle. Such reservoirs remain stable during a period comparable to the age of the Earth, and their height and width are comparable to those obtained with regular pPv. This result is consistent with previous studies showing that the most important parameters which control the stability and structure of the primordial reservoirs in the lower mantle are buoyancy ratio and thermal viscosity contrast [e.g., *McNamara and Zhong*, 2005; *Deschamps and Tackley*, 2009]. The presence of weak pPv, however, induces small differences.

Regarding the temperature field, we find that mantle cooling is slower with weak pPv, and the CMB heat flux is larger but more time dependent, because the weak pPv enhances the convective vigor above the CMB, which is consistent with previous studies [e.g., *Bower et al.*, 2009; *Tosi et al.*, 2010; *Nakagawa and Tackley*, 2011; *Samuel and Tosi*, 2012]. Cold slabs spread more widely along the CMB in the case with weak pPv. This tends to push the primordial reservoirs aside, sharpening the edges of these reservoirs and triggering the generation of hot upwellings from their margins.

Cadek and Fleitout [2006] pointed out that the viscosity of some cold downwelling regions may be less than the average, while hot regions are more viscous than average. Because plumes rise from these hot regions, plume dynamics may be altered by this situation. However, the 2-D Cartesian models of *Cizkova et al.* [2010] in 2-D Cartesian geometry show that this does not substantially modify the dynamics of the hot regions. Our calculations confirm this conclusion in 3-D spherical geometry. The hot primordial reservoirs also appear to be more viscous than the cold surrounding regions due to the low viscosity of pPv. This slightly strengthens the stability of these reservoirs and tends to generate a sharper boundary, but it does not prevent the growth and rise of plumes at the top of the hot reservoirs.

Our conclusions may be altered by several parameters. First, tomographic observations show clear evidence that the subducting slabs can reach the core-mantle boundary and may bring mid-ocean ridge basalt (MORB) to the lower mantle. Although in this study the size of primordial reservoirs does not change significantly, the study by *Nakagawa and Tackley* [2011] pointed out that the amount of recycled MORB segregating above the CMB might substantially increases due to the weak viscosity of the pPv. It is necessary to carefully examine the effect of weak pPv in a system which contains both primordial material and recycled MORB. Second, a large Clapeyron slope (e.g., 13 MPa/K) avoids a large or fully covering layer of pPv above CMB, but it may allow the phase change from Pv to pPv to occur within hot reservoirs of primordial material [*Lay et al.*, 2006; *Tackley et al.*, 2013]. This may trigger small-scale heterogeneities (e.g., ultralow velocity zones) in the lower mantle, whose effect on the stability of the dense reservoirs needs to be investigated. The temperature at the CMB may also play an important role. Here we used $T_{CMB} = 3750$ K based on the upper bound estimated by a recent mineral physics research by *Nomura et al.* [2014]. Higher temperatures, as previously estimated, would reduce the stability field of pPv. This would not alter the main conclusion that the stability of reservoirs of dense material is not affected by the presence of weak pPv. Finally, the potential effects of core cooling are not considered in this study. Core cooling, however, may alter the results from this study by leading to a faster cooling of the mantle due to the thermal effects induced by a weak pPv (e.g., higher CMB heat flux). As a consequence, after 4.5 Gyr the mantle temperature may be lower for the weak pPv case than for the regular pPv. This may in turn promote the formation of more pPv and potentially have a stronger influence on the stability of the reservoirs of dense material.

Acknowledgments
We are grateful to the Editor, Michael Wysession, and the two reviewers, Nicola Tosi and Mingming Li, for their constructive reviews. This work was supported by Swiss National Science Foundation grants SNF 200021-129510 and 200020-1496259 and Academia Sinica (Taipei, Taiwan) grant AS-102-CDA-M02. Calculations were run on ETH's Brutus cluster. All the data for this paper can be made available upon request from the authors.

Michael Wysession thanks Mingming Li and Nicola Tosi for their assistance in evaluating this paper.

References

Ammann, M., J. Brodholt, J. Wookey, and D. Dobson (2010), First-principles constraints on diffusion in lower-mantle minerals and a weak D" layer, *Nature*, *465*(7297), 462–465, doi:10.1038/nature09052.

Bower, D. J., M. Gurnis, J. M. Jackson, and W. Sturhahn (2009), Enhanced convection and fast plumes in the lower mantle induced by the spin transition in ferropericlase, *Geophys. Res. Lett.*, *36*, L10306, doi:10.1029/2009GL037706.

Burke, K., B. Steinberger, T. H. Torsvik, and M. A. Smethurst (2008), Plume generation zones at the margins of large low shear velocity provinces on the core-mantle boundary, *Earth Planet. Sci. Lett.*, *265*(1-2), 49–60, doi:10.1016/j.epsl.2007.09.042.

Cadek, O., and L. Fleitout (2006), Effect of lateral viscosity variations in the core-mantle boundary region on predictions of the long-wavelength geoid, *Stud. Geophys. Geod.*, *50*(2), 217–232, doi:10.1007/s11200-006-0013-0.

Christensen, U. R., and D. A. Yuen (1985), Layered convection induced by phase transitions, *J. Geophys. Res.*, *90*(B12), 10,291–10,300.

Cizkova, H., O. Cadek, C. Matyska, and D. A. Yuen (2010), Implications of post-perovskite transport properties for core-mantle dynamics, *Phys. Earth Planet. Inter.*, *180*(3-4), 235–243, doi:10.1016/j.pepi.2009.08.008.

Cobden, L., I. Mosca, J. Trampert, and J. Ritsema (2012), On the likelihood of post-perovskite near the core-mantle boundary: A statistical interpretation of seismic observations, *Phys. Earth Planet. Inter.*, *210-211*, 21–35, doi:10.1016/j.pepi.2012.08.007.

Davies, D. R., S. Goes, J. Davies, B. Schuberth, H.-P. Bunge, and J. Ritsema (2012), Reconciling dynamic and seismic models of Earth's lower mantle: The dominant role of thermal heterogeneity, *Earth Planet. Sci. Lett.*, *353-354*, 253–269, doi:10.1016/j.epsl.2012.08.016.

Deschamps, F., and P. J. Tackley (2008), Searching for models of thermo-chemical convection that explain probabilistic tomography: I. Principles and influence of rheological parameters, *Phys. Earth Planet. Inter.*, *171*(1-4), 357–373, doi:10.1016/j.pepi.2008.04.016.

Deschamps, F., and P. J. Tackley (2009), Searching for models of thermo-chemical convection that explain probabilistic tomography. II—Influence of physical and compositional parameters, *Phys. Earth Planet. Inter.*, *176*(1-2), 1–18, doi:10.1016/j.pepi.2009.03.012.

Deschamps, F., L. Cobden, and P. J. Tackley (2012), The primitive nature of large low shear-wave velocity provinces, *Earth Planet. Sci. Lett.*, *349-350*, 198–208, doi:10.1016/j.epsl.2012.07.012.

He, Y., and L. Wen (2012), Geographic boundary of the "Pacific Anomaly" and its geometry and transitional structure in the north, *J. Geophys. Res.*, *117*, B09308, doi:10.1029/2012JB009436.

Hernlund, J. W. (2010), On the interaction of the geotherm with a post-perovskite phase transition in the deep mantle, *Phys. Earth Planet. Inter.*, *180*(3-4), 222–234, doi:10.1016/j.pepi.2010.02.001.

Hernlund, J. W., C. Thomas, and P. J. Tackley (2005), A doubling of the post-perovskite phase boundary and structure of the Earth's lowermost mantle, *Nature*, *434*(7035), 882–886.

Hofmann, A. (1997), Mantle geochemistry: The message from oceanic volcanism, *Nature*, *385*(6613), 219–229, doi:10.1038/385219a0.

Ishii, M., and J. Tromp (1999), Normal-mode and free-air gravity constraints on lateral variations in velocity and density of Earth's mantle, *Science*, *285*(5431), 1231–1236, doi:10.1126/science.285.5431.1231.

Kageyama, A., and T. Sato (2004), "Yin-yang grid": An overset grid in spherical geometry, *Geochem. Geophys. Geosyst.*, *5*, Q09005, doi:10.1029/2004GC000734.

Labrosse, S., J. Hernlund, and N. Coltice (2007), A crystallizing dense magma ocean at the base of the Earth's mantle, *Nature*, *450*(7171), 866–869.

Lay, T., J. Hernlund, E. J. Garnero, and M. S. Thorne (2006), A post-perovskite lens and D" heat flux beneath the central Pacific, *Science*, *314*(5803), 1272–1276, doi:10.1126/science.1133280.

Lee, C.-T. A., P. Luffi, T. Höink, J. Li, R. Dasgupta, and J. Hernlund (2010), Upside-down differentiation and generation of a primordial lower mantle, *Nature*, *463*(7283), 930–933, doi:10.1038/nature08824.

Li, M., and A. K. McNamara (2013), The difficulty for subducted oceanic crust to accumulate at the Earth's core-mantle boundary, *J. Geophys. Res. Solid Earth*, *118*, 1807–1816, doi:10.1002/jgrb.50156.

Li, Y., F. Deschamps, and P. J. Tackley (2014), The stability and structure of primordial reservoirs in the lower mantle: Insights from models of thermochemical convection in three-dimensional spherical geometry, *Geophys. J. Int.*, *199*(2), 914–930, doi:10.1093/gji/ggu295.

Masters, G., G. Laske, H. Bolton, and A. Dziewonski (2000), The relative behavior of shear velocity, bulk sound speed, and compressional velocity in the mantle: Implications for chemical and thermal structure, in *Earth's Deep Interior: Mineral Physics and Tomography From the Atomic to the Global Scale, Geophys. Monog. Ser.*, vol. 117, edited by S.-I. Karato et al., pp. 63–87, AGU, Washington, D. C.

McNamara, A. K., and S. Zhong (2005), Thermochemical structures beneath Africa and the Pacific Ocean, *Nature*, *437*(7062), 1136–1139.

Mosca, I., L. Cobden, A. Deuss, J. Ritsema, and J. Trampert (2012), Seismic and mineralogical structures of the lower mantle from probabilistic tomography, *J. Geophys. Res.*, *117*, B06304, doi:10.1029/2011JB008851.

Murakami, M., K. Hirose, K. Kawamura, N. Sata, and Y. Ohishi (2004), Post-perovskite phase transition in MgSiO3, *Science*, *304*(5672), 855–858, doi:10.1126/science.1095932.

Nakagawa, T., and P. J. Tackley (2011), Effects of low-viscosity post-perovskite on thermo-chemical mantle convection in a 3-D spherical shell, *Geophys. Res. Lett.*, *38*, L04309, doi:10.1029/2010GL046494.

Ni, S., E. Tan, M. Gurnis, and D. Helmberger (2002), Sharp sides to the African superplume, *Science*, *296*(5574), 1850–1852, doi:10.1126/science.1070698.

Nomura, R., K. Hirose, K. Uesugi, Y. Ohishi, A. Tsuchiyama, A. Miyake, and Y. Ueno (2014), Low core-mantle boundary temperature inferred from the solidus of pyrolite, *Science*, *343*(6170), 522–525, doi:10.1126/science.1248186.

Oganov, A. R., and S. Ono (2004), Theoretical and experimental evidence for a post-perovskite phase of MgSiO3 in Earth's D" layer, *Nature*, *430*(6998), 445–448.

Samuel, H., and N. Tosi (2012), The influence of post-perovskite strength on the Earth's mantle thermal and chemical evolution, *Earth Planet. Sci. Lett.*, *323-324*, 50–59, doi:10.1016/j.epsl.2012.01.024.

Sidorin, I., M. Gurnis, and D. V. Helmberger (1999), Dynamics of a phase change at the base of the mantle consistent with seismological observations, *J. Geophys. Res.*, *104*(B7), 15,005–15,023.

Solomatov, V. S., and D. J. Stevenson (1993), Suspension in convective layers and style of differentiation of a terrestrial magma ocean, *J. Geophys. Res.*, *98*(E3), 5375–5390, doi:10.1029/92JE02948.

Tackley, P. J. (2008), Modelling compressible mantle convection with large viscosity contrasts in a three-dimensional spherical shell using the yin-yang grid, *Phys. Earth Planet. Inter.*, *171*(1-4), 7–18, doi:10.1016/j.pepi.2008.08.005.

Tackley, P. J., T. Nakagawa, and J. W. Hernlund (2013), Influence of the post-perovskite transition on thermal and thermo-chemical mantle convection, in *Post-Perovskite: The Last Mantle Phase Transition, Geophys. Monogr. Ser.*, vol. 174, edited by K. Hirose et al., pp. 229–247, AGU, Washington, D. C., doi:10.1029/174GM16.

Tateno, S., K. Hirose, N. Sata, and Y. Ohishi (2009), Determination of post-perovskite phase transition boundary up to 4400 k and implications for thermal structure in d layer, *Earth Planet. Sci. Lett.*, *277*(1-2), 130–136, doi:10.1016/j.epsl.2008.10.004.

Torsvik, T. H., M. A. Smethurst, K. Burke, and B. Steinberger (2006), Large igneous provinces generated from the margins of the large low-velocity provinces in the deep mantle, *Geophys. J. Int.*, *167*(3), 1447–1460, doi:10.1111/j.1365-246X.2006.03158.x.

Tosi, N., D. A. Yuen, and O. Čadek (2010), Dynamical consequences in the lower mantle with the post-perovskite phase change and strongly depth-dependent thermodynamic and transport properties, *Earth Planet. Sci. Lett.*, *298*(1-2), 229–243, doi:10.1016/j.epsl.2010.08.001.

Trampert, J., F. Deschamps, J. Resovsky, and D. Yuen (2004), Probabilistic tomography maps chemical heterogeneities throughout the lower mantle, *Science*, *306*(5697), 853–856, doi:10.1126/science.1101996.

Tsuchiya, T., J. Tsuchiya, K. Umemoto, and R. M. Wentzcovitch (2004), Phase transition in MgSiO3 perovskite in the Earth's lower mantle, *Earth Planet. Sci. Lett.*, *224*(3-4), 241–248, doi:10.1016/j.epsl.2004.05.017.

Wang, Y., and L. Wen (2007), Geometry and P and S velocity structure of the "African Anomaly," *J. Geophys. Res.*, *112*, B05313, doi:10.1029/2006JB004483.

Wookey, J., S. Stackhouse, J.-M. Kendall, J. Brodholt, and G. D. Price (2005), Efficacy of the post-perovskite phase as an explanation for lowermost-mantle seismic properties, *Nature*, *438*(7070), 1004–1007.